

# Broad resonances and beta-decay

K. Riisager<sup>a,\*</sup>, H.O.U. Fynbo<sup>a</sup>, S. Hyldegaard<sup>a</sup>, A.S. Jensen<sup>a</sup>

<sup>a</sup>*Department of Physics and Astronomy, Aarhus University, DK-8000 Aarhus C, Denmark*

---

## Abstract

Beta-decay into broad resonances gives a distorted lineshape in the observed energy spectrum. Part of the distortion arises from the phase space factor, but we show that the beta-decay matrix element may also contribute. Based on a schematic model for p-wave continuum neutron states it is argued that beta-decay directly to the continuum should be considered as a possible contributing mechanism in many decays close to the driplines. The signatures in R-matrix fits for such decays directly to continuum states are discussed and illustrated through an analysis of the beta-decay of  ${}^8\text{B}$  into  $2^+$  states in  ${}^8\text{Be}$ .

---

## 1. Introduction

The concept of a resonance is pervasive in quantum physics as applied e.g. on nuclear, particle, atomic and molecular phenomena. However, a closer look at the literature shows that there is no unique way of defining a resonance. When applied in data analysis, varying definitions can give different results for broad resonances [1, 2, 3] or may even at some point become impossible to apply. There are two distinct aspects of a resonance, the first being as a state of a (continuum) system in analogy with a bound state, the second as characterizing an enhanced response to a disturbance. We shall here mainly be concerned with the first aspect.

We shall focus in this paper on beta-delayed particle emission processes that traditionally are considered to proceed through (resonance) states in the beta-decay daughter and shall argue that beta-decays directly to the continuum should be taken into account in more situations than done so far. Before dealing specifically with beta-decay we shall in section 2 remind the reader about some aspects of the description of resonances and how well they perform when applied to broad resonances. This will be illustrated in

---

\*Corresponding author, [kvr@phys.au.dk](mailto:kvr@phys.au.dk)

section 3 through simple model calculations. One goal is to clarify whether parameters taken from analyses of beta-decay data can be used in modelling of other nuclear processes proceeding through the same “reaction channels”, we show in section 4 that loosely bound initial states may require special considerations. In the limit of very broad resonances it is not possible to decouple the population of the resonance from its decay. The properties of the resonance, its position and width (or more generally its shape), will differ when populated via different mechanisms. Since analyses of decays through broad levels are often made via R-matrix fits we shall discuss (section 4.3) what effects may occur there. Finally, section 5 discusses how our results may be generalized and section 6 presents our conclusion.

It may be appropriate first to recall that a resonance as such does not correspond directly to any physical observable. However, the resonance concept can be very useful in describing the evolution of a system, e.g. as a response to an external probe, namely by employing resonances as basis states in the description. We are of course never forced to use a specific set of basis states, but narrow resonances in particular seem a natural choice. In the opposite limit of very broad structures the alternative description in terms of “pure” continuum states (a basis defined by the asymptotic behaviour of the wavefunctions) may seem the natural one. It is important to note that both descriptions are valid and, at least for structures of intermediate width, can be used in practice. A practical example can be found in the calculation [4] of the dipole strength function for  $^{11}\text{Be}$  where a basis combining resonances and continuum contributions is used and it is demonstrated explicitly how the number of included resonances can be varied without changing the result. (The complex scaling method [5] used in this work can be related to the Berggren decomposition of the continuum [6, 7].)

From such general considerations it appears that it is to some extent a matter of convenience whether one interprets an experimental spectrum in terms of resonances or not. This point has been made very clearly by Dalitz [8, 9]. The two possible descriptions, emphasizing resonances or continuum states, may be thought of as complementary, and the question of whether a process happens resonantly or not will as noted earlier [10, 11] not always have a unique, or meaningful, answer. Nevertheless it is worthwhile to explore how far the resonance concept may be taken, to see how different resonance definitions relate to experimental observables, and to determine when corrections must be included.

## 2. Limits for resonant behaviour

Most resonance definitions are conceptual or formal, but do agree in the case of narrow resonances. Resonances may also be identified in experimental spectra, and a standard requirement has been that several different observables should give consistent (energy and width) parameters for a given resonance, the point being that resonances should be an intrinsic property of the system studied and ideally not influenced by the ways of exciting it. For increasingly broader resonances the deduced parameters can no longer be expected to be identical for the different conceptual definitions or different observables.

Blatt and Weisskopf [12] start their exposition of nuclear resonances by considering the relative amplitude of wavefunctions inside and outside the nucleus. A resonance corresponds to an enhancement of the interior wavefunction and thereby to a spatial concentration. Another possibility is to look at the time delay between incoming and outgoing wave packets that should be large, see eg. [8, 13]. That these two criteria are equivalent is shown by the discussion in [14] on how the presence of an unstable state leads to localization. As  $\Gamma$  (the resonance width parameter) increases these two ways of identifying resonances become less clear: the enhancement of the interior wavefunction for a given energy will decrease and the delay time (lifetime) will approach the transit time of the constituents across the nucleus.

It is well known that a state decaying exponentially in time will have an energy distribution given by a Breit-Wigner shape, but this distribution can also be derived in several other ways, see e.g. [12, 13, 14, 15]. For broad levels the pure Breit-Wigner shape has to be corrected (energy distributions do not extend below zero energy, nor to arbitrarily high energies). Furthermore it becomes harder to unambiguously interpret broad structures in energy spectra as (distorted) Breit-Wigner distributions since bumps in an energy distribution may occur for a number of other reasons [8, 9].

When following the evolution of a bound state as its energy is increased and crosses the threshold to the continuum, it is tempting to extend the eigenvalue description by employing complex energies and letting the state acquire an imaginary energy corresponding to half its width. One often in theoretical descriptions starts from complex eigenstates with purely outgoing waves, the Gamow states [16]. This naturally leads to the description of resonances as poles (at complex values) in the S-matrix [13, 17]. This is the definition employed in most, but not all [18], treatments in mathematical physics. It leads to very elegant formulations, but also runs into problems for very broad states. On one hand, as pointed out by Sitenko [19], the assumption of purely outgoing waves is no longer realistic when the time delay is very

short. On the other hand, as noted e.g. in [13], we can easily identify poles close to the real axis in experimental data (that are on the real axis), but as widths become larger and the poles move away from the real axis it becomes increasingly harder to make this identification. In practical situations one often has to introduce more than one state and thereby many parameters for the states to determine from the experimental spectrum, examples will be given in section 4.3. In the extreme situation there is “more input from the theoretical skeleton than from the experimental data”.

See also [9, 20, 21, 22, 23, 24, 25, 26, 27] for more (and complementary) accounts of the resonance phenomenon.

### 3. Schematic model

The changes that occur as resonances become broader will be illustrated in a schematic model where the many nuclear degrees of freedom are restricted to the motion of a single neutron. The corresponding strong potential is taken to be a square well with radius  $a = 4$  fm and depth  $V_0 > 0$ . For a positive energy  $E = (\hbar k)^2/2\mu$  (for definiteness we shall take the reduced mass  $\mu$  to be 10/11 of the neutron mass) and an angular momentum  $l$  the radial wavefunction,  $R(r)$ , inside the potential is proportional to  $j_l(Kr)$  where  $E + V_0 = (\hbar K)^2/2\mu$ . Outside the potential the radial wavefunction is normalized to be the linear combination  $[\cos \delta_l j_l(kr) - \sin \delta_l y_l(kr)]k$  of the regular and irregular spherical Bessel function of order  $l$ . Here  $\delta_l$  is the phase shift that is found by matching the inner and outer wavefunction. The explicit factor of  $k$  implies that the wavefunction is normalized to approach  $\sin(kr + \delta_l - l\pi/2)/r$  for large radii  $r$ . We shall mainly consider p-waves, this is the simplest case where resonances occur since s-waves that have no confining potential form virtual states instead.

#### 3.1. Elastic scattering

This simple model will now be used to compare different resonance definitions. First of all, a phase shift that goes through  $\pi/2$  is often used as a criterion. This is closely related to elastic scattering for which the cross section is

$$\sigma_l = \frac{\pi}{k^2} (2l + 1) |e^{2i\delta_l} - 1|^2 . \quad (1)$$

The factor  $|e^{2i\delta_l} - 1| = 2 \sin \delta_l$  is clearly maximal when the phase shift equals  $\pi/2 + n\pi$ . However, for broad levels the variation of the front factor  $k^{-2}$  shifts down the maximum for the cross section to lower energies. As a second way to define resonances, one may look at the enhancement of the interior wavefunction that can be quantified through the integral  $I = \int_0^a |R(r)|^2 r^2 dr$

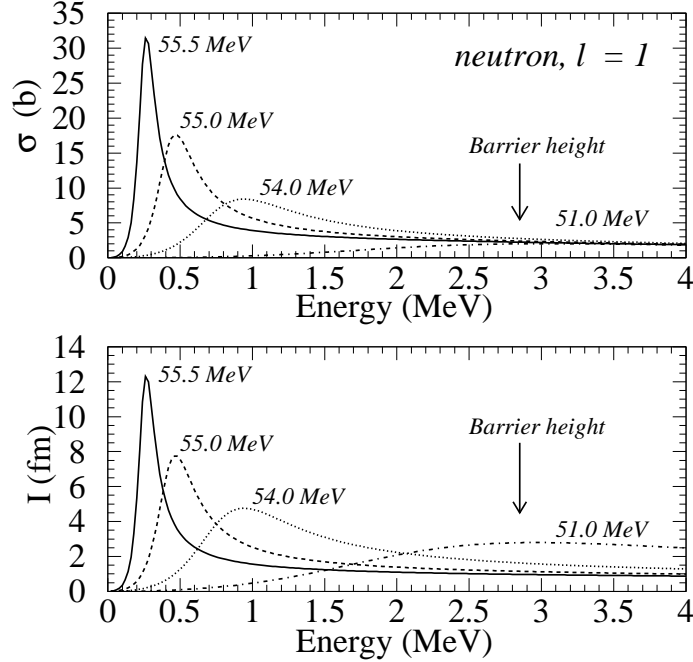


Figure 1: Upper panel: Elastic cross-section, lower panel: the integral of the squared wavefunction inside the potential. Both are calculated for p-wave neutrons in a square well of radius 4.0 fm and shown as a function of energy for different well depths as marked in the figure. The height of the angular momentum barrier is marked by an arrow.

of the squared wavefunction over the potential range. If no potential is present, i.e. the neutron is in an s-wave and  $V_0 = 0$  MeV, the integral averages to  $a/2 = 2$  fm.

Figure 1 shows the calculated elastic cross-section  $\sigma$  and the integral  $I$  of the interior wavefunction as a function of energy for different choices of the potential depth  $V_0$  just above 50 MeV (in this range there will be one bound state in the potential). As seen in the figure peaks occur as long as they are well below the height of the potential barrier. The peak shape of both  $\sigma$  and  $I$  become wide and asymmetric as the peak positions increase, note that the peak positions and widths are quite similar in the two cases. There is still a broad structure visible in  $I$  for  $V_0 = 51.0$  MeV, but a less clear signal in  $\sigma$ . Furthermore, the positions where the phase shift goes through  $\pi/2$  deviates more and more from the visual peak and the phase shift never reaches  $\pi/2$  for potential depth 51.0 MeV. The resonance positions according to these two definitions are given in table 1 in column two and four. The peak position

Table 1: The position of a resonance for p-wave neutrons in a square well of radius 4 fm and depth  $V_0$  according to four different definitions: the total or resonant phase shift,  $\delta_l$  or  $\delta_R$ , going through  $\pi/2$  and the maxima of the elastic cross-section or the beta-strength distribution. All energies are in units of MeV.

$V_0$	Resonance energy			
	$\delta_l = \frac{\pi}{2}$	$\delta_R = \frac{\pi}{2}$	$\max \sigma_l$	$\max B(E)_{E_i=1\text{MeV}}$
55.5	0.278	0.276	0.266	0.256
55.0	0.510	0.497	0.469	0.436
54.5	0.791	0.748	0.693	0.616
54.0	1.146	1.028	0.942	0.797
53.0	2.358	1.672	1.518	1.154
52.0	–	2.411	2.216	1.500
51.0	–	3.219	3.05	1.831
12.0	0.975	0.894	0.814	0.705
11.5	1.379	1.177	1.055	0.868
11.0	1.970	1.486	1.314	1.027

for the integral  $I$  is essentially identical to the position of the maximum of the elastic scattering cross section. The lower part of table 1 have potential depths corresponding to wavefunctions with no nodes inside the potential, for the upper part there is one node.

### 3.2. A second look at resonance definitions

The numerical results shown above suggests that resonances should be characterized by being localized in space as well as peaked in energy, this seems natural for the case of short-ranged potentials considered in this paper. The implications of this point of view will be pursued in the following sections, but a few observations can be made already.

The enhancement of the wavefunction inside the potential will also be present in the region just outside. The integral  $I^{out} = \int_a^{2a} |R(r)|^2 r^2 dr$  will in most cases be larger than  $I$  for states of energy close to the peak energy. This will be important when we shall consider transition matrix elements in the next section, but it also underlines that resonance wavefunctions do differ qualitatively from bound state wavefunctions. An exception to this is halo states that also extend significantly beyond the potential range.

The wavefunction inside the potential,  $j_l(Kr)$  in our model, changes explicitly with energy through  $K$ . The relative change across a peak of width  $\Gamma$  is easily shown to be  $\Delta K/K = \Gamma/2/(E + V_0)$  and can become appreciable for very broad states. In this limit both the normalization and the functional shape of the interior resonance wavefunction is no longer unique. This situation can be contrasted to the one encountered in R-matrix theory that is

often used in advanced analyses of experimental data. We refer to [15, 28, 29] for a full account of R-matrix theory and only summarize the main features here: Internal levels  $\lambda$  appear from quantization within the channel radius  $a_c$ , they have energies  $E_\lambda$  and amplitude  $\gamma_\lambda$  for coupling to a decay channel. The internal wavefunctions form a discrete basis set for the interior, but the levels cannot automatically be identified as resonances, we shall elaborate on this in section 4.3. For the cases where such an identification can be made Lane and Thomas showed in section XII.2 of their review [28] that for an internal wavefunction  $\Psi$  formed with unit incoming flux (spherical wave) one has at a resonance for the integral over the internal region:

$$\int |\Psi|^2 d^3r = \frac{\hbar\Gamma_\lambda}{(E_\lambda + \Delta - E)^2 + \Gamma_\lambda^2/4}, \quad (2)$$

where  $\Gamma_\lambda = 2P\gamma_\lambda^2$ ,  $\Delta = -(S - B)\gamma_\lambda^2$ , the penetrability and shift factor for the channel,  $P$  and  $S$ , are energy dependent and the boundary parameter  $B$  normally is set equal to  $S$  at resonance. This explicitly shows how the single-level (Breit-Wigner) resonance formula is related to our integral  $I$ . If one here approximates  $S$  by a linear function (section XII.3 of [28]) one obtains an expression with “observed” parameters rather than the above, more formal R-matrix parameters:

$$C \frac{\hbar\Gamma_0}{(E_0 - E)^2 + \Gamma_0^2/4}, \quad C = \frac{1}{1 + \gamma_\lambda^2 dS/dE}, \quad (3)$$

where now  $\Gamma_0 = C\Gamma_\lambda$  corresponding to a renormalization of  $\gamma_\lambda^2$  and  $E_0 = E_\lambda + \Delta$ . However, the energy dependence of the penetrability implies that the maximum of the distribution may be shifted away from  $E_0$  [30]. In the limit of small shifts one can for neutrons derive that the maximum is positioned at

$$E_{max} = E_0 \left[ 1 - \alpha \left( \frac{\Gamma_0}{4E_0} \right)^2 \right], \quad (4)$$

where the parameter  $\alpha$  for a given angular momentum  $l$  increases from 1 far above the barrier to  $2l + 1$  well below the barrier. For p-waves  $\alpha = [3 + (ka)^2]/[1 + (ka)^2]$ .

For an isolated resonance the phase shift in R-matrix theory consists of two contributions  $\delta_l = \phi_l + \delta_R$ . Here  $\phi_l = \tan^{-1}(j_l/y_l)$  is the hard sphere phase shift and

$$\delta_R = \tan^{-1} \left( \frac{\Gamma_\lambda/2}{E_\lambda + \Delta - E} \right) \quad (5)$$

is the contribution from the resonance. Since the resonance position in R-matrix theory is defined by  $E_\lambda + \Delta - E = 0$  it corresponds to  $\delta_R$  being  $\pi/2$ .

The corresponding resonance positions have been evaluated and are also given as the third column in table 1. (The final column will be explained in the next section.) Using  $\delta_R$  rather than  $\delta_l$  clearly gives more appropriate resonance positions; the increase of more than one MeV in  $\delta_l$ -resonance position as  $V_0$  is decreased from 54 MeV to 53 MeV is not sensible. For broad resonances  $\delta_R$  gives a resonance position above the peak position, but this result actually depends on the value chosen for the channel radius  $a_c$  used to evaluate  $\phi_l$ . It was here taken equal to  $a = 4$  fm, but increasing it to 6 fm will move the extracted resonance positions down e.g. to 0.477 MeV and 1.380 MeV for  $V_0 = 55$  MeV and 53 MeV. This highlights one of the conceptual problems in R-matrix theory, namely the possible dependence of results on the channel radius, see e.g. the discussion in [29]. We shall return to the question of resonance positions extracted from R-matrix theory in section 4.3.

#### 4. Beta-delayed neutron emission

Beta-decay may populate broad resonances, in particular in light nuclei, and could conceptually present a new angle on the issue since one here enters “abruptly” into a strongly interacting system, thereby circumventing Sitenko’s point presented above. Broad resonances could therefore appear differently when populated in beta decay rather than in nuclear reactions. Population through gamma decays (or photo-dissociation) will be similar, but with a slightly more complex operator. Although there are fewer detailed studies of gamma decays to broad levels, some exist [31, 32, 33] and related studies on photo-dissociation processes can also be relevant. References to the extensive literature on beta decay to continuum levels may be found e.g. through a recent review paper [34].

##### 4.1. Model calculations

The operator for allowed beta-decay transforms a neutron into a proton without further changes to the wavefunction. This is approximated in the schematic model by assuming that a core nucleon is transformed. The neutron is then involved through the overlap matrix element between an initial state bound p-wave neutron (with a binding energy  $E_i$  that can be varied) and the above final state continuum p-wave function. With our normalization of the latter wavefunction the matrix element has dimension of a length, and the phase space factor corresponding to the density of final neutron states is  $2/(\pi\hbar v)$  where  $v = \hbar k/\mu$  is the velocity (the factor can be derived from the more detailed expressions in [35]). We follow [36] and define the differential beta-strength  $B(E)$  as the product of the matrix element squared and the neutron phase space factor. The beta-decay rate,  $w(E)$ , at a given energy



$E$  is then proportional to  $f(Q - E)B(E)$  where  $f$  is the usual beta-decay phase space factor. The  $f$ -factor has a substantial energy dependence which will move the observed peak position by roughly  $-(5/8)\Gamma_0^2/(Q - E_0)$ , see [36] for details. We shall here focus on the behaviour of  $B(E)$  and note that the  $f$ -factor can be divided out from experimental data so that its effects can be removed. We neglect for the moment any effects of non-perfect overlap in the core, but return below to a more detailed discussion of the assumptions made.

For initial neutron states that are well bound so that the wavefunction is mainly inside the potential one could expect the square of the overlap matrix element to be similar to the integral  $I$  from the previous section. However, the beta-strength contains an extra factor  $1/v$  that will move the peak position down and reduce its width. This can be seen in the upper panel of figure 2 by comparing the (rescaled) elastic cross-section with the differential beta-strength for a 5 MeV initial state (dotted line). For initial states with smaller binding energy the wavefunction will extend beyond the potential and there will be a contribution to the overlap matrix element also from the external region. This leads to a further shift of the peak position and modification of the line shape as shown in figure 2. The area under the curves is the same (due to the beta-decay strength sum rule), and the strength is moved from higher energies to lower energies thereby shifting the peak downwards, for the very low initial binding energy of 20 keV a low-energy shoulder develops. These changes may be understood as follows. Less initial binding energy  $E_i$  gives a wavefunction with slower radial fall-off which increases the importance of the external contribution. This enhances the overlap for final state energies  $E$  of order and smaller than  $E_i$ , but when  $E$  increases the oscillations in the final state wavefunction become more rapid and the overlap is suppressed. It must be stressed that all changes seen in figure 2 for different  $E_i$  are due to the structure of the initial state. The final state continuum is exactly the same in all calculations.

The lower panel of the figure also shows schematic results corresponding to  $(\gamma, n)$  dissociation reactions with E1 transitions. The initial states are here taken as neutron s-waves of different energy, and the matrix element now includes a factor  $r$  as appropriate for the E1 operator. The quantity plotted is the matrix element squared times  $2/(\pi\hbar v)$ . The extra factor of  $r$  in the matrix elements (and the fact that the initial s-wave neutron state can be more extended than a p-wave) enhances the effects mentioned above, but the overall qualitative behaviour is similar. One can include the external electromagnetic contributions explicitly in a resonance framework such as R-matrix theory (see section XIII.3 in [28]), as also extended by Barker to the

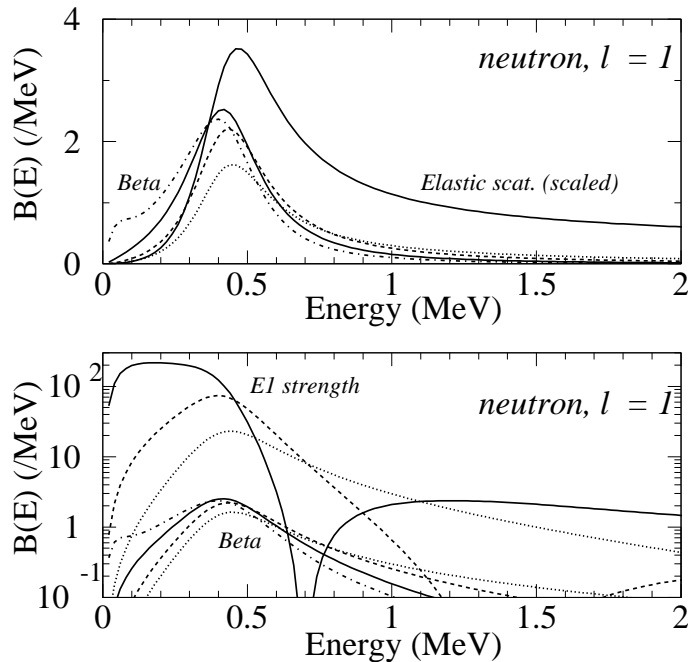


Figure 2: The beta-strength to a p-wave neutron continuum for a square well radius 4.0 fm and potential depth 55.0 MeV is shown as a function of energy. Initial state binding energy is 5.0 MeV (dotted line), 1.0 MeV (dashed line), 0.2 MeV (solid line) and 0.02 MeV (dash-dotted line), respectively. Upper panel also shows the elastic cross-section (in barn) scaled down by a factor 5. Lower panel also shows the E1 strength for initial s-wave states with binding energies 5.0 MeV, 1.0 MeV and 0.2 MeV.

case of beta-decays<sup>1</sup> [37], but for the radiative capture case ( $(n,\gamma)$ , the inverse reaction to dissociation) it is customary to speak in terms of a direct capture process, see e.g. [40]. For the E1 results in figure 2 we would therefore speak of a transition from a resonance dominated to a direct transition dominated process as  $E_i$  is reduced. With the similar, but less pronounced, tendencies in beta decay we may in a similar way attribute the changes to an increasing contribution from decays directly into the continuum as  $E_i$  is decreased.

It is worth stressing that we are dealing with two limits of the same physical process rather than two distinct reaction mechanisms. For the case of E1 transitions the direct and resonant dominated limits clearly correspond

<sup>1</sup>Barker pointed out that this may be equivalent to considering processes with inverse time ordering [38, 39], where the particle emission happens before the beta decay.

to the main contributions coming from external distances and internal distances, respectively. It does not make much sense to attempt to define a strict borderline between the two limits, to give just one example a resonance may give clear interference effects for processes that are mainly due to direct contributions. Before leaving the electromagnetic processes it should be noted that the drastic effects seen here are at least partly due to the initial s-states. At low binding energies these are halo states, see e.g. [41], and it is well established [42, 43] that their pronounced low-energy E1-strength is non-resonant.

The maxima of the  $B(E)$  distributions are also given in table 1 for the case of initial binding energy  $E_i$  of 1 MeV. The shift down in energy with respect to the maximum of the elastic cross-section is sizeable in all cases, although always below a “half width at half maximum”. The resonances appearing in our model calculation have single-particle strength by construction. One can reduce the width of the resonances by introducing an extra delta-shell potential. We have checked that doing this reduces the overall scale of the energy shifts, but peak shifts are still present with a similar magnitude of the peak shift to peak width ratio. If on the other hand the beta strength is significantly smaller than unity (the single-particle value) the beta transition may be due to other, and smaller, components in the initial wavefunction where the effective binding energies are larger. In this case the dependence on  $E_i$  will be strongly reduced.

To further illustrate the effects that may occur in beta decay, two extreme cases are shown in figure 3, namely the final state potential of 51.0 MeV that in figure 1 gave broad structure around the barrier height, and the case where the final state potential vanishes. In the former case the effect of the initial state binding energy is very high, shifting the peak position by more than 1 MeV and giving significantly narrower distributions. In the latter case there are no resonances and the beta strength can only be attributed to direct transitions to the continuum. More than 50% of the beta strength sum rule value appears below 10 MeV for all shown cases with no nodes in the initial wavefunction.

Since beta-decay gives resonance-like shapes even in rather extreme situations, it is of interest to see also the behaviour for an s-wave neutron continuum. Here the elastic scattering has a cross-section that decreases monotonically, one talks of a virtual state rather than a resonance and characterizes it by a scattering length  $a_s$ . The four panels in figure 4 show results for beta-decays into such an s-wave continuum with scattering lengths decreasing from 30 fm to 3 fm (the corresponding energy scales  $\hbar^2/(2\mu a_s^2)$  go from 2.5 keV to 2.5 MeV). There is now a distinct difference in the beta-strength distributions obtained for different initial state binding energies,

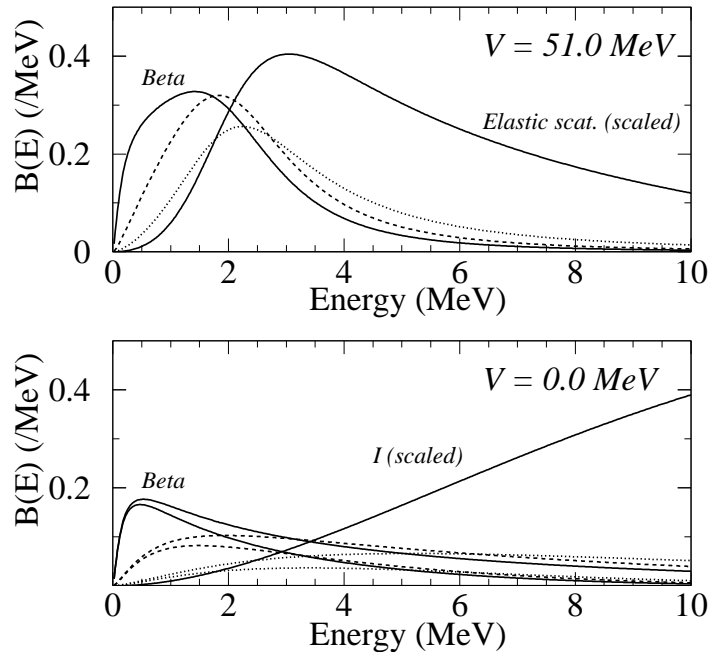


Figure 3: The beta-strength to a p-wave neutron continuum for a square well radius 4.0 fm and potential depth 51.0 MeV (upper panel) or 0.0 MeV (lower panel). Initial state binding energy is 5.0 MeV (dotted line), 1.0 MeV (dashed line) and 0.2 MeV (solid line), respectively. Upper panel also shows the elastic cross-section (in barn) scaled down by a factor 5. Lower panel also shows the integral  $I$  of the squared wavefunction over the interior scaled down by a factor 4. The two sets of beta-strength curves in the lower panel are for initial wavefunctions with no (upper curves) and one (lower curves) node inside the potential.

the figure gives results from 0.2 MeV (a clear halo state) to 5 MeV (close to standard binding energy). Still, all distributions peak at low energy (at a position that depends as much on the scattering length as on the initial binding energy) and have a pronounced asymmetric shape with a long tail towards high energies. The tail is less extended for smaller initial binding energies since the spatially larger initial wavefunction gives rise to a quicker cancellation in the overlap matrix element. Most of the beta strength (for 1 MeV initial binding energy more than 98% of the sum rule) is lying between 0 MeV and 10 MeV. The shape of the distributions is not really resonance-like, but varies significantly less than the elastic scattering cross-sections.

In summary, beta-decay may clearly distort the shape of a resonance. The dependence of the beta-strength on the initial state is a threshold effect,

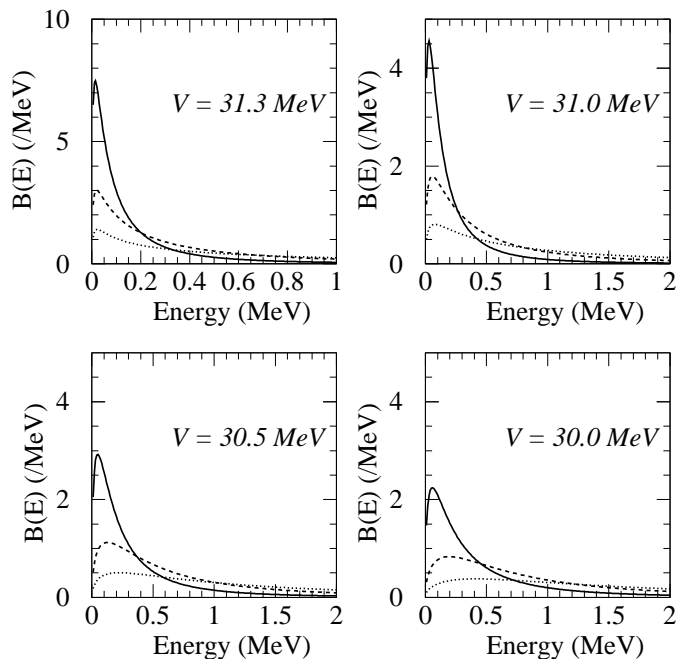


Figure 4: The beta-strength to an s-wave neutron continuum for a square well radius 4.0 fm and potential depths as marked in the four panels. The corresponding scattering lengths are 30 fm, 14 fm, 6.1 fm and 3.0 fm, respectively. The initial state binding energy is 5.0 MeV (dotted line), 1.0 MeV (dashed line) and 0.2 MeV (solid line), respectively. Note that the upper left panel has different ranges than the other panels.

occurring when the initial binding energy is so low that wavefunctions extend in a significant manner outside of the nuclear core. It affects both peak position and peak shape and appears even for an s-wave continuum. The binding energy dependence may be reduced for transitions with low beta strength, but the distortion with respect to elastic scattering should remain for very broad resonances. It is interesting to compare this with the detailed calculations of continuum-continuum E2 transitions in  $^8\text{Be}$  discussed in [44]. In that case contributions to the transition matrix element were found to arise mainly from the short distance region. One may expect net contributions from larger distances to appear only for continuum-continuum transitions where both initial and final state have small  $k$ -values.

#### 4.2. Applicability of the model

In the calculations above the beta-decay takes place in the core whereas the initial neutron bound in a p-wave goes into a continuum p-wave state.

The model is clearly schematic and may exaggerate the effect in that it has both maximum beta decay strength and full single-particle strength for the subsequent particle emission. The interesting effects happen at low neutron binding and we are therefore dealing with  $\beta^-$  decays. To have a final state with good isospin we need to add a component where the core is unchanged and the p-wave neutron is transformed into a proton. In the usual core plus single-particle model (see e.g. section 3-1 in [10]) the component that we consider here with an unchanged neutron is the main one in the isobaric analogue state (IAS) and the minor one in the state of lower isospin. We shall consider the applicability of the model separately for Fermi and Gamow-Teller transitions, but note that the model could be appropriate for M1 excitations where the spin part is dominating.

Standard  $\beta^-$  decay does not populate the IAS (except for the neutron and triton), but neutrino scattering ( $\nu_e, e$ ) may do so in a Fermi transition. Still, the Coulomb energy keeps the neutron threshold with the appropriate isospin above the IAS so that it only decays by neutron emission through isospin impurities. To get a Fermi contribution to beta-delayed neutron emission two conditions must be met. First, the spatial overlap between the initial state and the IAS must be less than one. This will happen if the initial and final potentials differ slightly so that the two states have different binding energy measured from their respective thresholds. Experimentally such differences can be of order 100 keV; our simple model in such cases gives feeding to the continuum of order one percent for binding energies less than 1 MeV. (With exactly the same potential in initial and final state there is of course no continuum feeding.) The second condition is that isospin conservation is broken. Large effects can only be expected for the low-lying continuum where the asymmetry of the Coulomb effects is most noticeable. In the schematic model decays only take place via the component where the core is beta-decaying and the requirement is therefore that the core final state is unbound. This can be achieved when the starting configuration is a two-neutron halo,  $^{11}\text{Li}$  being the classic example. A more detailed investigation of how large fraction of the Fermi strength could realistically reside in the low-lying continuum would be very interesting, the current model is clearly not applicable but suggests that the one percent level is not out of reach.

For Gamow-Teller transitions the beta strength will be reduced due to the fact that the component we consider now is a small part of a transition, but this is partly compensated by the factor 3 from the spin operator. The model may therefore be thought of as a schematic model for beta-delayed neutron emission from nuclei with the last filled neutrons in p-orbits. An interesting case is the beta decay of  $^{14}\text{Be}$  where the largest branch goes to a state [45, 46, 47] fed with a Gamow-Teller strength close to 1 and situ-

ated about 300 keV above the one neutron threshold in  $^{14}\text{B}$ . The beta-decay experiments report a neutron line of energy 288(1) keV (corresponding to a level 308 keV above threshold) and width 49(2) keV, but a somewhat asymmetric line shape. A later  $^{14}\text{Be}(p,n)^{14}\text{B}$  reaction experiment at 69 MeV [48] reported a transition corresponding to a level 304(4) keV above threshold and a substantially larger width of 160(20) keV. Even without detailed calculations of the charge exchange reaction mechanism the difference in width seems too large to be accounted for in our model: for a potential depth of 55.4 MeV elastic scattering will have a peak position at 305 keV and a FWHM of 204 keV (a single-particle strength), while for an initial binding energy in the range 0.5-1.0 MeV the beta strength will have a peak position around 15 keV lower and a FWHM around 170 keV. Nevertheless, a more detailed investigation of this case would be very interesting.

Two possible cases occur for the neutron-rich boron isotopes, although in both cases for transitions with beta strength of order 0.1 or less. The nucleus  $^{13}\text{B}$  decays into a  $1/2^-$  8.860(20) MeV level in  $^{13}\text{C}$  with width 150(30) keV [49]; here the latest published experiment [50] is from 1974 and did not give accurate energies for the position of the level. A recent experiment [51] on the beta decay of  $^{17}\text{B}$  found indications for a 2.5(7) MeV wide 5.04(2) MeV neutron line tentatively attributed to neutron emission from a level at 6.08 MeV in  $^{17}\text{C}$ . If this is confirmed one can in any case expect large effects for a resonance that is so wide. Other relevant examples may be the decays of nuclei such as  $^8\text{He}$ ,  $^9\text{Li}$  or heavier nuclei around  $^{50}\text{K}$ .

Similar effects to the ones exposed here may occur also in other beta-delayed particle emission processes. Before discussing that it is useful to look at how R-matrix fits behave in our model.

#### 4.3. *R-matrix fits*

R-matrix theory allows to include effects such as the penetrability and interference that can alter the spectral shape for broad resonances. It is therefore often employed in fits of experimental data in order to extract parameter values. We shall test here what happens for our model calculations for the case of  $V_0 = 55$  MeV. For the phase shifts equation (5) gives an almost perfect fit to the data when the hard sphere phase shift is evaluated and the fit performed for  $a_c = a = 4$  fm. The resonance position is at 0.497 MeV and the  $\gamma_\lambda$  parameter corresponds to a total level width equal to a single particle unit (the Wigner limit). If  $a_c$  is chosen as 6 fm (and the hard sphere phase shift corrected accordingly) it is not possible to produce an acceptable fit with one resonance, to get this one needs to introduce a second level or add a constant background term to the R-matrix.

Table 2: Results of R-matrix fits to beta strength distributions for potential depth 55.0 MeV. All energies are in units of MeV.

$E_i$	$E_{max}$	FWHM	$E_1$	$\Gamma_1$	$B_1$	$E_2$	$\Gamma_2$	$B_2$
0.2	0.41	0.30	0.45	0.38	0.44	360	8.0	$4.8 \cdot 10^5$
1.0	0.44	0.31	0.48	0.40	0.40	499	$1.1 \cdot 10^4$	78
5.0	0.45	0.33	0.49	0.41	0.31	39	1.21	282

We have furthermore fitted the calculated  $B(E)$  distributions for initial state binding energies of 0.2 MeV, 1.0 MeV and 5.0 MeV shown in figure 2. A fit with a single level did not produce acceptable fits even though the channel radius was set to 4 fm. The results for fits with two levels are displayed in table 2, the agreement between calculated and fitted distribution is perfect for the 5.0 MeV data, but there are systematic deviations for the other two energies. The table gives the observed position and full width at half maximum (in MeV) for the three  $B(E)$  distributions as well as the R-matrix “observed” values [28, 29] of the energies  $E_i$ , the widths  $\Gamma_i$  and the beta strength parameters  $B_i$  for transitions to the two levels.

It is interesting that the differences in the maximum of the distribution,  $E_{max}$ , are seen as well in the extracted fit values for  $E_1$ . The shift of  $E_{max}$  relative to  $E_1$  is close to that given by equation (4). However, the shape of the distributions necessitated the two component fits where in all cases the two R-matrix levels interfere destructively between the two level positions. The width parameters  $\Gamma_1$  therefore do not correspond to the observed FWHM values and the beta strength parameters  $B_1$  are lower than the maximum value of one. The parameters of the second level are poorly constrained by the data and the fit uncertainties therefore large. Nevertheless, the parameters  $B_2$  are in all cases unrealistically large, as is also the case for several values of  $E_2$  and  $\Gamma_2$ . The overall fit can therefore not be interpreted in terms of physically well-defined resonances, it rather resembles the situation encountered in the R-matrix fits [52] to the decay of  $^{12}\text{N}$  into states in  $^{12}\text{C}$  above the alpha particle threshold where unphysical values of  $E$ ,  $\Gamma$  and  $B$  were obtained when a  $0_4^+$  level was introduced in the fits (this was done in order to reach an acceptable  $\chi^2$ -value).

Adding more levels in the R-matrix fit may in principle lead to a more acceptable solution, but the extra parameters introduced as levels are added implies that it will not be possible to determine all parameters solely from the data. The contribution from the regions outside of the nuclear core that occur in beta decay for small initial binding energy can therefore be expected to give a difference in extracted resonance energy between analyses of beta decay and elastic scattering data. In our example this difference reached



more than 10% of the width of the level.

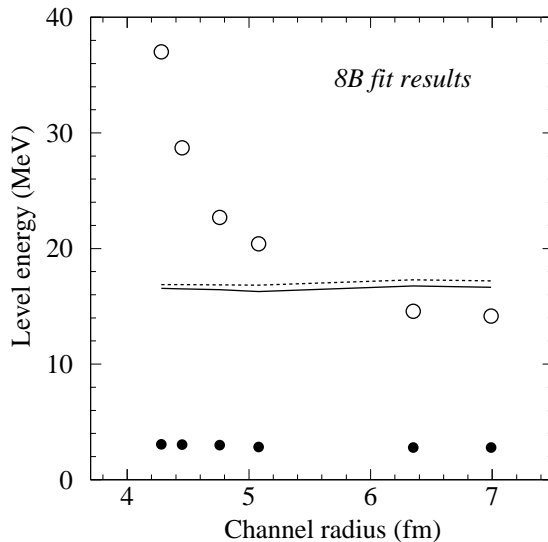


Figure 5: The observed energies of the fitted levels from an R-matrix four-level fit [54] of the beta-delayed alpha-spectrum from the decay of  ${}^8\text{B}$  is shown versus the channel radius used for the fit. The positions of the well established 3 MeV level (filled circle) and the  $2^+$  doublet close to 17 MeV (lines) are stable whereas the position of the fourth level (open circle) varies.

To learn more about how R-matrix fits may be interpreted we turn to the example of the beta-delayed alpha decay of  ${}^8\text{B}$  which has been studied on several occasions. We use the spectrum obtained recently in [53] that also gives details on earlier work as well as a brief account of the fitting procedure and results for a fit with channel radius 4.5 fm. More details on the fit as well as results for other channel radii can be found in [54]. To get an acceptable fit one needs to include, apart from the well established level at 3 MeV and the  $2^+$  doublet at 16.6 MeV and 16.9 MeV, a fourth  $2^+$  level, see figure 5 that shows the energy positions as function of channel radius. The nature of the extra level has been discussed on several occasions, see e.g. [55, 56, 57, 58], with Barker arguing from a simultaneous fit to scattering and decay data that it is an intruder state. However, not all R-matrix levels can be interpreted as resonances [15, 28, 59]. For the case of  ${}^8\text{Be}$  a detailed demonstration of this was made for the s-wave resonances in a comparison [60] of R-matrix and K-matrix fits.

In more general terms this was demonstrated already by Wigner and Eisenbud [59] who showed how R-matrix theory treats even the case of van-

ishing interaction through an infinite number of levels  $i$  with parameters  $E_i = \hbar^2/(2M)(2i - 1)^2(\pi/(2a_c))^2$  and  $\gamma_i = (-1)^i\sqrt{\hbar^2/(Ma_c)}$ . These levels cannot be interpreted as resonances, but are needed in order to reproduce the case of “no scattering”. They do appear since the R-matrix levels form a complete set of basis functions. If, as is often the case, a small number of R-matrix levels is used in a fit one may find the need for a “background level” with unphysical energies or  $\gamma$ -parameter, such a level effectively incorporates the effects of the above infinite number of levels, as illustrated in [60]. Turning this around, to incorporate continuum behaviour in an R-matrix fit one needs extra levels with large  $\gamma$  values and approximate distance

$$E_{i+1} - E_i = \frac{\hbar^2\pi^2}{Ma_c^2}i. \quad (6)$$

(The value for  $a_c = 5$  fm and  $i = 1$  is 8.25 MeV for the alpha-alpha system and 18.0 MeV for the neutron system above.) The fourth level in figure 5 has a dependence on the channel radius  $a_c$  that is consistent with this behaviour and indeed has quite large values of  $\gamma$  (clearly larger than the ones for the 3 MeV level, and therefore unphysical) and may therefore function as an effective level. One would expect that introducing more levels in the fits would give better behaviour, in particular at large  $a_c$ , but the alternative approach that interprets the need for such extra levels as a signature of a noticeable direct contribution seems more attractive. That fits performed at large channel radii may need more levels is consistent with the general practice [29] of using rather small values for the radii.

In summary, R-matrix theory has a complete basis and can reproduce any decay mechanism, also decays directly to continuum states. The presence of such decays can be indicated in several ways: by R-matrix levels that do not correspond to any physical “bump” in the spectra, by level energies that scale inversely as the channel radius squared, or by levels that have unphysically large values for the parameters that represent the coupling to different channels, like  $\gamma$  and  $B$ .

## 5. Discussion

### 5.1. Other beta-delayed decays

Most beta-delayed neutron emissions will not proceed through states with single-particle neutron strength. The delta-shell potential introduced above to mimic this effect may not be sufficiently realistic, but the observed dependence on the initial state binding energy should remain and could in extreme cases give peak shifts approaching the width of the resonance.

The mirror process is proton emission following  $\beta^+$  decay. The Coulomb barrier will now affect both initial and final proton states and diminish the contribution from distances beyond the nuclear potential. On the other hand more decay channels will be open, there is e.g. beta-feeding to the IAS for nuclei with more protons than neutrons. A special situation may be encountered for isospin 1 systems where (in light nuclei) the nuclei with isospin projection  $\pm 1$  can both decay to the same states in the nucleus with projection 0. These mirror decays may now differ in line shape. Two possible cases occur for isospin 3/2 systems: The beta decay of  $^{13}\text{O}$  includes a transition to a level at 8.198 keV in  $^{13}\text{N}$  that is more than 200keV wide, this is the mirror transition to the  $^{13}\text{B}$  case considered earlier. The proton energy has only been measured in one experiment [61] where a surprising energy shift 50 keV upwards with respect to reaction data was reported. A more careful investigation of this case seems needed. The beta decay of  $^{17}\text{Ne}$  includes a transition to a quite broad, 700(250) keV, 8.2 MeV  $3/2^-$  level [62, 63] but the energy of this resonance has not been measured precisely in any experiment.

The main remaining beta-delayed process to consider is beta-delayed alpha decay (delayed emission of other particles, such as tritons, has also been observed, but only in rather few nuclei). For such transitions the overlap integrals will be more complex and simple models hardly adequate. Nevertheless, there are, as alluded to above, experimental data that may point to related effects. Consider first the decays of  $^8\text{B}$  and  $^8\text{Li}$  into  $2^+$  levels in  $^8\text{Be}$  that subsequently decay by breaking up into two alpha particles. As shown in the previous section the most natural explanation of the  $^8\text{B}$  decay data is in terms of a contribution also from direct decays to continuum states. A detailed comparison of peak positions of the lowest  $2^+$  resonance in the two decays and in alpha-alpha scattering performed in [58] gave the same value within about 20 keV, but the beta strength is low in this case so the expected energy shift may be small. Furthermore, the beta decay strength parameters for the two mirror decays differed in the analysis and it may be worthwhile to try to model the system rather than relying on R-matrix fits.

As the next example, consider decays leading to the alpha-particle cluster states in  $^{12}\text{C}$  where the R-matrix fits mentioned above [52] also strongly indicated the presence of decays directly to the continuum. Here one is dealing with a three alpha particle final state which further complicates the theoretical treatment. Existing cluster models [64, 65] may be a starting point for an analysis, but in order also to evaluate the overlap integrals that enter in the beta-decay process they have to be extended.

Finally, the E1 component of the astrophysically important  $^{12}\text{C}(\alpha,\gamma)^{16}\text{O}$  reaction is often evaluated by combining reaction and beta decay data, see e.g. [66, 67]. In the combined fit to data the resonance position and width

is assumed to be the same for all processes. In view of our results this assumption should be checked.

### 5.2. Other experimental probes

It would be interesting to extend the calculations also to other ways of populating resonances in order to see how large difference may be there. A good starting point for transfer reactions could be the semiclassical model for transfer to continuum states by Bonaccorso and Brink [35]. Coupled channels calculations may also be used to treat inelastic scattering. For knockout reactions at higher beam energies there is already an extensive discussion on the reaction mechanism, see e.g. [68] where arguments for a dominance of direct transitions are presented.

It was striking to see the rather large difference in spectral shape between elastic scattering and beta-decay that appeared for very wide structures (to some extent even for s-wave systems), a difference that must arise from the fact that the initial state in beta decay is confined. This suggests that beta-decay is more sensitive to broad resonances than elastic scattering. It will be interesting to see how other experimental probes will behave and whether there will be similar effects of spatially extended nuclear states (e.g. the rather loosely bound deuteron often employed in transfer reactions). We have so far only considered allowed beta-decay. In higher orders,  $\lambda$ , one encounters matrix elements that, similar to the case of electromagnetic interactions, involve spherical Bessel functions  $j_\lambda(qr)$  (or their generalization to take into account the effects of the nuclear Coulomb field) with a wave number  $q$  in the relevant range for the transition [10]. This will lead to an enhancement of direct transitions similar to that already mentioned for electromagnetic transitions. The same conclusion also holds for processes at somewhat higher energy, such as electron or neutrino scattering or muon capture [69], where the higher order processes become more important.

### 5.3. The non-resonant continuum ?

When calculating processes close to a threshold and employing a framework, such as the Gamow Shell Model [70], that is sufficiently powerful to capture both bound state and continuum behaviour, results are sometimes described in terms of resonant and non-resonant continuum contributions. Such a division is of course, as practitioners are well aware, only possible with a specific choice of which resonances are included; the example of the calculation of the  $^{11}\text{Be}$  dipole strength function [4] was quoted already. A distinction may be made within a theoretical model, but one cannot find a

general and unambiguous experimental way of separating resonant and non-resonant processes. This is well established (see e.g. appendix 3F in [10]), but the above calculations illustrate this in a new way.

The terms resonant and non-resonant continuum suggests that it is a property of the continuum, i.e. of the final state on its own. The cases discussed above where the initial state structure influenced the detailed line shape shows that such an interpretation can lead to a rather complex description of actual processes. In a similar way radiative capture can in limiting cases be described as proceeding through resonant capture or direct capture, but will in general have contributions from both, and a general distinction between one reaction mechanism and the other cannot be made. Assuming as in section 3.2 that a resonance should be localized in configuration space as well as in energy, one may use short-distance and large-distance contributions as ways of distinguishing resonant and continuum terms; see e.g. the explicit discussion in [44] where cross terms also appeared, but note that the exact point of division is arbitrary.

Based on the picture of spatial division one would distinguish resonant and non-resonant contributions through their different radial contribution. This explains why operators with different radial weighting have different sensitivities to “non-resonant” contributions, with electromagnetic transitions being more prone to display a direct mechanism. Except for situations where one of the two contributions dominate, a clear-cut division is not possible.

## 6. Conclusion

The most important features of broad resonances and our main results may be summarized as follows:

- In the limit of broad resonances, different ways of defining a resonance will not have the same range of validity and will not give the same values for the resonance position and width.
- Beta-decay (and to an even larger extent electromagnetic) transitions may get contributions from extra-nuclear distances, this distorts the observed line shape. The effect can be naturally interpreted as a contribution from decays directly to continuum states. In general such contributions will increase in importance as one approaches the driplines, partly due to the low binding energies occurring there, partly due to the fact that more transitions with large beta strength will be seen. Transitions with large beta strength are more likely to show an effect.

- Extraction of resonance parameters from data has to be done with care. The comparison of elastic scattering and beta-decay showed that R-matrix resonance parameters may depend on the process. R-matrix fits of continuum contributions require introduction of extra levels. Such levels often have unphysical parameter values: energies that depend on the channel radius or too strong coupling parameters.
- Combining information from different types of experiments in order to narrow down the properties of a resonance can therefore go wrong for broad levels. A concrete example of this is the  $2^+$  levels in  $^8\text{Be}$  discussed in section 4.3. Conversely, using resonance parameters from one experiment in another seemingly resonance dominated process may not be appropriate. In such cases a more involved theoretical analysis must be done.
- Different experimental probes differ in their sensitivity to resonance structure, beta-decay may be more sensitive than other probes such as elastic scattering. This is due to the initial state in beta-decay being localized.
- The levels that enter in R-matrix fits can not always be interpreted as resonances, the example discussed in detail involved the  $^8\text{B}$  decay.

Our results were obtained mainly for continuum p-wave neutrons, but the more complex case of continuum s-waves was also considered briefly. The trends found should persist for other beta-delayed particle emission processes and related cases, and some of our findings may also be relevant outside of nuclear physics for other systems with short-range potentials situated close to a threshold.

Acknowledgement. We would like to thank D.V. Fedorov and C.Aa. Diget for discussions.

## References

- [1] D.R. Tilley, C.M. Cheves, J.L. Godwin, G.M. Hale, H.M. Hofmann, J.H. Kelley, C.G. Sheu and H.R. Weller, Nucl. Phys. **A708** (2002) 3
- [2] Particle Data Group, K.A. Olive et al., Chin. Phys. C **38** (2014) 090001
- [3] A.R. Bohm and Y. Sato, Phys. Rev. **D71** (2005) 085018
- [4] T. Myo, A. Ohnishi and K. Kato, Prog. Theor. Phys. **99** (1998) 801

- [5] T. Myo, Y. Kikuchi, H. Masui and K. Kato, *Prog. Part. Nucl. Phys.* **79** (2014) 1
- [6] T. Berggren, *Nucl. Phys.* **A109** (1968) 265
- [7] T. Berggren and P. Lind, *Phys. Rev.* **C47** (1993) 768
- [8] R.H. Dalitz and R.G. Moorhouse, *Proc. Roy. Soc. Lond. A* **318** (1970) 279
- [9] S. Albeverio, L.S. Ferreira and L. Streit (Eds), “Resonances — Models and Phenomena” *Lecture Notes In Physics* 211 (Springer, 1984)
- [10] A. Bohr and B.R. Mottelson, *Nuclear Structure*, Vol. 1 (Benjamin, 1969)
- [11] G. Breit, *Rev. Mod. Phys.* **36** (1964) 1071
- [12] J.M. Blatt and V.F. Weisskopf, *Theoretical Nuclear Physics* (Wiley, 1952)
- [13] J.R. Taylor, *Scattering Theory* (Wiley, 1972)
- [14] L. Fonda, G.C. Ghirardi and A. Rimini, *Rep. Prog. Phys.* **41** (1978) 587
- [15] G. Breit, “Theory of resonance reactions and allied topics” *Encyclopedia of Physics (Handbuch der Physik)*, ed. S. Flügge (Springer, 1959) Vol 41/1
- [16] O. Civitarese and M. Gadella, *Phys. Reports* **396** (2004) 41
- [17] B. Simon, *Int. J. Quantum Chem.* **14** (1978) 529
- [18] A. Orth, *Commun. Math. Phys.* **126** (1990) 559
- [19] A.G. Sitenko, *Lectures in scattering theory* (Pergamon, 1971)
- [20] A.M. Badalyan, I.P. Kok, M.I. Polikarpov and Yu.A. Simonov, *Phys. Reports* **82** (1982) 31
- [21] N. Erlander, *Int. J. Quantum Chem.* **31** (1987) 707
- [22] Arno Böhm, *Quantum Mechanics*, 3rd edition (Springer, 1993)
- [23] N. Moiseyev, *Phys. Reports* **302** (1998) 211
- [24] F. Fernández-Alonso and R.N. Zare, *Ann. Rev. Phys. Chem.* **53** (2002) 67

- [25] J. Okołowicz, M. Płoszajczak and I. Rotter, Phys. Reports **374** (2003) 271
- [26] N. Hatano, Prog. Theor. Phys. Suppl. **184** (2010) 497
- [27] J. Carbonell, A. Deltuva, A.C. Fonseca and R. Lazauskas, Prog. Part. Nucl. Phys. **74** (2014) 55
- [28] A.M. Lane and R.G. Thomas, Rev. Mod. Phys. **30** (1958) 257
- [29] P. Descouvemont and D. Baye, Rep. Prog. Phys. **73** (2010) 036301
- [30] F. Barker, Proc. Phys. Soc. **84** (1964) 681
- [31] L. De Braekeleer, E.G. Adelberger, J.H. Gundlach, M. Kaplan, D. Markoff, A.M. Nathan, W. Schieff, K.A. Snover, D.W. Storm, K.B. Swartz, D. Wright and B. A. Brown, Phys. Rev. **C51** (1995) 2778
- [32] O.S. Kirsebom, M. Alcorta, M.J.G. Borge, M. Cubero, C.Aa. Diget, R. Dominguez-Reyes, L. Fraile, B.R. Fulton, H.O.U. Fynbo, D. Galaviz, G. Garcia, S. Hyldegaard, H.B. Jeppesen, B. Jonson, P. Joshi, M. Madurga, A. Maira, A. Muñoz, T. Nilsson, G. Nyman, D. Obradors, A. Perea, K. Riisager, O. Tengblad and M. Turrion, Phys. Lett. **B680** (2009) 44
- [33] V.M. Datar, D.R. Chakrabarty, Suresh Kumar, V. Nanal, S. Pastore, R.B. Wiringa, S.P. Behera, A. Chatterjee, D. Jenkins, C.J. Lister, E.T. Mirgule, A. Mitra, R.G. Pillay, K. Ramachandran, O.J. Roberts, P.C. Rout, A. Shrivastava and P. Sugathan, Phys. Rev. Lett. **111** (2013) 062502
- [34] M. Pfützner, M. Karny, L.V. Grigorenko and K. Riisager, Rev. Mod. Phys. **84** (2012) 567
- [35] A. Bonaccorso and D.M. Brink, Phys. Rev. **C38** (1988) 1776
- [36] K. Riisager, Nucl. Phys. **A925** (2014) 112; *ibid* **A925** (2014) 298
- [37] F.C. Barker, Phys. Lett. **B322** (1994) 17
- [38] T.A. Griffy and L.C. Biedenharn, Nucl. Phys. **15** (1960) 636
- [39] M.J.G. Borge, L. Johannsen, B. Jonson, T. Nilsson, G. Nyman, K. Riisager, O. Tengblad and K. Wilhelmsen Rolander, Nucl. Phys. **A560** (1993) 664
- [40] A.M. Lane and J.E. Lynn, Nucl. Phys. **17** (1960) 563



- [41] A.S. Jensen, K. Riisager, D.V. Fedorov and E. Garrido, *Rev. Mod. Phys.* **76** (2004) 215
- [42] T. Otsuka, M. Ishihara, N. Fukunishi, T. Nakamura and M. Yokayama, *Phys. Rev.* **C49** (1994) R2289
- [43] T. Aumann and T. Nakamura, *Phys. Scr.* **T152** (2013) 014012
- [44] E. Garrido, A.S. Jensen and D.V. Fedorov, *Phys. Rev.* **C88** (2013) 024001
- [45] M. Belbot, J. J. Kolata, M. Zahar, N. Aoi, M. Hirai, M. Ishihara, H. Okuno, H. Sakurai, T. Teranishi, T. Kishida, G. Liu, T. Nakamura, Y. Watanabe, A. Yoshida, E. Ideguchi, H. Miyatake, S. Shimoura, and S.S. Yamamoto, *Phys. Rev.* **C56** (1997) 3038
- [46] H. Jeppesen, U.C. Bergmann, M.J.G. Borge, J. Cederkäll, V.N. Fedoseyev, H.O.U. Fynbo, V.Y. Hansper, B. Jonson, K. Markenroth, V.I. Mishin, T. Nilsson, G. Nyman, K. Riisager, O. Tengblad and K. Wilhelmsen Rolander, *Nucl. Phys.* **A709** (2002) 119
- [47] N. Aoi, K. Yoneda, E. Ideguchi, T. Kishida, T. Nakamura, M. Notani, H. Sakurai, T. Teranishi, Y. Watanabe, H. Wu, A. Yoshida, H. Miyatake, Y. Yamamoto, H. Ogawa, S. S. Yamamoto, and M. Ishihara, *Phys. Rev.* **C66** (2002) 014301
- [48] Y. Satou, T. Nakamura, Y. Kondo, N. Matsui, Y. Hashimoto, T. Nakabayashi, T. Okumura, M. Shinohara, N. Fukuda, T. Sugimoto, H. Otsu, Y. Togano, T. Motobayashi, H. Sakurai, Y. Yanagisawa, N. Aoi, S. Takeuchi, T. Gomi, M. Ishihara, S. Kawai, H.J. Ong, T.K. Onishi, S. Shimoura, M. Tamaki, T. Kobayashi, Y. Matsuda, N. Endo, M. Kitayama, *Phys. Lett.* **B697** (2011) 459
- [49] F. Ajzenberg-Selove, *Nucl. Phys.* **A523** (1991) 1
- [50] D.E. Alburger and D.R. Goosman, *Phys. Rev.* **C10** (1974) 935
- [51] H. Ueno, H. Miyatake, Y. Yamamoto, S. Tanimoto, T. Shimoda, N. Aoi, K. Asahi, E. Ideguchi, M. Ishihara, H. Izumi, T. Kishida, T. Kubo, S. Mitsuoka, Y. Mizoi, M. Notani, H. Ogawa, A. Ozawa, M. Sasaki, T. Shirakura, N. Takahashi, and K. Yoneda, *Phys. Rev.* **C87** (2013) 034316
- [52] S. Hyldegaard, M. Alcorta, B. Bastin, M.J.G. Borge, R. Boutami, S. Brandenburg, J. Büscher, P. Dendooven, C.Aa. Diget, P. Van Duppen,

- T. Eronen, S.P. Fox, L.M. Fraile, B.R. Fulton, H.O.U. Fynbo, J. Huikari, M. Huyse, H.B. Jeppesen, A.S. Jokinen, B. Jonson, K. Jungmann, A. Kankainen, O.S. Kirsebom, M. Madurga, I. Moore, A. Nieminen, T. Nilsson, G. Nyman, G.J.G. Onderwater, H. Penttilä, K. Peräjärvi, R. Raabe, K. Riisager, S. Rinta-Antila, A. Rogachevskiy, A. Saastamoinen, M. Sohani, O. Tengblad, E. Traykov, Y. Wang, K. Wilhelmsen, H.W. Wilschut and J. Äystö, *Phys. Rev.* **C81** (2010) 024303
- [53] O.S. Kirsebom, S. Hyldegaard, M. Alcorta, M.J.G. Borge, J. Büscher, T. Eronen, S. Fox, B.R. Fulton, H.O.U. Fynbo, H. Hultgren, A. Jokinen, B. Jonson, A. Kankainen, P. Karvonen, T. Kessler, A. Laird, M. Madurga, I. Moore, G. Nyman, H. Penttilä, S. Rahaman, M. Reponen, K. Riisager, T. Roger, J. Ronkainen, A. Saastamoinen, O. Tengblad and J. Äystö, *Phys. Rev.* **C83** (2011) 065802
- [54] S. Hyldegaard, PhD thesis, Aarhus University (2010), unpublished
- [55] E.K. Warburton, *Phys. Rev.* **C33** (1986) 303
- [56] F.C. Barker, *Aust. J. Phys.* **42** (1989) 25
- [57] P.R. Page, *Phys. Rev.* **C72** (2005) 054312
- [58] M. Bhattacharya, E.G. Adelberger and H.E. Swanson, *Phys. Rev.* **C73** (2006) 055802
- [59] E.P. Wigner and L. Eisenbud, *Phys. Rev.* **72** (1947) 29
- [60] J. Humblet, A. Csótó and K. Langanke, *Nucl. Phys.* **A638** (1998) 714
- [61] H.H. Knudsen, H.O.U. Fynbo, M.J.G. Borge, R. Boutami, P. Dendooven, C.Aa. Diget, T. Eronen, S. Fox, L.M. Fraile, B. Fulton, J. Huikari, H.B. Jeppesen, A.S. Jokinen, B. Jonson, A. Kankainen, I. Moore, A. Nieminen, G. Nyman, H. Penttilä, K. Riisager, S. Rinta-Antila, O. Tengblad, Y. Wang, K. Wilhelmsen, and J. Äystö, *Phys. Rev.* **C72** (2005) 044312
- [62] M.J.G. Borge, H. Cronberg, M. Cronqvist, H. Gabelmann, P.G. Hansen, L. Johannsen, B. Jonson, S. Mattsson, G. Nyman, A. Richter, K. Riisager, O. Tengblad, M. Tomaselli, *Nucl. Phys.* **A490** (1988) 287
- [63] A.C. Morton, J.C. Chow, J.D. King, R.N. Boyd, N.P.T. Bateman, L. Buchmann, J.M. D’Auria, T. Davinson, M. Dombisky, W. Galster, E. Gete, U. Giesen, C. Iliadis, K.P. Jackson, J. Powell, G. Roy, A. Shotter, *Nucl. Phys.* **A706** (2002) 15

- [64] R. Roth, T. Neff, H. Feldmeier, Prog. Part. Nucl. Phys. **65** (2010) 50
- [65] Y. Kanada Eny'o, Prog. Theor. Phys. **117** (2007) 655
- [66] L. Buchmann, G. Ruprecht and C. Ruiz, Phys. Rev. **C80** (2009) 045803
- [67] D. Schürmann, L. Gialanella, R. Kunz and F. Strieder, Phys. Lett. **B711** (2012) 35
- [68] E. Garrido, D.V. Fedorov, A.S. Jensen and K. Riisager, Phys. Rev. Lett. **86** (2001) 1986
- [69] N.T. Zinner, K. Langanke and P. Vogel, Phys. Rev. **C74** (2006) 024326
- [70] J. Dobaczewski, N. Michel, W. Nazarewicz, M. Płoszajczak, J. Rotureau, Prog. Part. Nucl. Phys. **59** (2007) 432